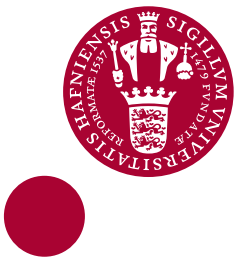

The structure of the serotonin system

A PET imaging study

Beliveau, Vincent; Ozenne, Brice; Strother, Stephen; Greve, Douglas N.; Svarer, Claus; Knudsen, Gitte Moos; Ganz, Melanie

Published in:
NeuroImage

DOI:
10.1016/j.neuroimage.2019.116240

Publication date:
2020

Document version
Publisher's PDF, also known as Version of record

NeuroImage 205 (2020) 116240

Contents lists available at ScienceDirect

NeuroImage

journal homepage: www.elsevier.com/locate/neuroimage

The structure of the serotonin system: A PET imaging study

Vincent Beliveau [a], Brice Ozenne [a,d], Stephen Strother [e], Douglas N. Greve [f,g], Claus Svarer [a], Gitte Moos Knudsen [a,c], Melanie Ganz [a,b,*]

[a] Neurobiology Research Unit, Copenhagen, Denmark
[b] Department of Computer Science, University of Copenhagen, Copenhagen, Denmark
[c] Faculty of Health and Medical Sciences, University of Copenhagen, Copenhagen, Denmark
[d] Section of Biostatistics, University of Copenhagen, Copenhagen, Denmark
[e] Rotman Research Institute, Baycrest, and Department of Medical Biophysics, University of Toronto, Toronto, Canada
[f] Athinoula A. Martinos Center for Biomedical Imaging, Department of Radiology, Massachusetts General Hospital, Boston, MA, USA
[g] Harvard Medical School, Boston, MA, USA

ARTICLE INFO

Keywords:
Serotonin
PET
MRI
Clustering
Structure
mRNA

ABSTRACT

The human brain atlas of the serotonin (5-HT) system does not conform with commonly used parcellations of neocortex, since the spatial distribution of homogeneous 5-HT receptors and transporter is not aligned with such brain regions. This discrepancy indicates that a neocortical parcellation specific to the 5-HT system is needed. We first outline issues with an existing parcellation of the 5-HT system, and present an alternative parcellation derived from brain MR- and high-resolution PET images of five different 5-HT targets from 210 healthy controls. We then explore how well this new 5-HT parcellation can explain mRNA levels of all 5-HT genes. The parcellation derived here represents a characterization of the 5-HT system which is more stable and explains the underlying 5-HT molecular imaging data better than other atlases, and may hence be more sensitive to capture region-specific changes modulated by 5-HT.

1. Introduction

Serotonin (5-hydroxytryptamine, 5-HT) plays a central role in the regulation and function of the human brain. The modulatory effects of 5-HT are broad and extensive and are implicated in highly diverse aspects of brain physiology and pathology, such as the regulation of sleep and major depression. For an in-depth review of the brain functions and disorders related to the 5-HT system see (Muller and Jacobs, 2009). This rich versatility is reflected in the diversity of receptors composing the 5-HT system; with 7 families of receptors (5-HT_1 to 5HT_7) consisting of 14 subtypes and a transporter (5-HTT), the 5-HT system is one of the most complex receptor systems linked to a single neurotransmitter. Whereas the distribution of a subset of the 5-HT receptors and the 5-HT transporter in the human brain has been well characterized through autoradiography (Varnäs et al., 2004), and more recently *in vivo* (Beliveau et al., 2017; Savli et al., 2012), the regions describing the spatial distribution of receptor density across receptor types have been largely unexplored.

From the early work on its cytoarchitectonic structure (Broadman, 1909), the brain is known to be organized in coherent, specialized regions. In vivo molecular neuroimaging of the 5-HT system with Positron Emission Tomography (PET) is most often assessed on the basis of atlases derived from the anatomical structure of the brain (Desikan et al., 2006; Svarer et al., 2005; Kalbitzer and Svarer, 2009; Tzourio-Mazoyer et al., 2002). In the absence of further knowledge about the spatial structure of the 5-HT system, these anatomical atlases constitute a reasonable assumption about the spatial organization of this system. However, there is no evidence that the distribution of 5-HT targets (receptors and transporter) accurately follows the regions presented in these atlases. On the contrary, the regional variation in 5-HT targets found in a high resolution *in vivo* 5-HT atlas (Beliveau et al., 2017) suggests that the 5-HT system may have its own underlying spatial organization consisting of regions of homogeneous receptor density. Indeed, a structural atlas derived from the cortical gyri and sulci of the human brain, such as the Desikan-Killiany (DK) atlas (Desikan et al., 2006), may be inadequate to explain the organization of the 5-HT system as its regions contain a spatially inhomogeneous concentration of the 5-HT targets (Beliveau et al., 2017).

A parcellation of the 5-HT system based on PET neuroimaging data from 108 healthy individuals has recently been presented in James et al.

* Corresponding author. Neurobiology Research Unit, Copenhagen, Denmark.
E-mail address: mganz@nru.dk (M. Ganz).

https://doi.org/10.1016/j.neuroimage.2019.116240
Received 25 April 2019; Received in revised form 26 September 2019; Accepted 1 October 2019
Available online 7 October 2019

(2018). Although this parcellation likely captures the main regions involved in the 5-HT system, we are concerned that it shows patterns similar to partial volume effects (PVE) observed in surface-based analysis of PET data (Greve et al., 2014). Furthermore, the clustering strategy proposed by James and colleagues may lead to unstable parcellations due to the chosen clustering approach. Finally, the dataset used to derive the clustering presented in their analysis also included PET data for Monoamine Oxidase A (MAO-A), an enzyme which degrades all amine neurotransmitters and is not specific to the 5-HT system.

We propose an alternative approach which uses a watershed-type algorithm to perform the clustering which regularizes the parcellations by using spatial information. Furthermore, our dataset is acquired on a high resolution PET scanner, additionally consists of the 5-HT_{1B} and the 5-HT_4 receptors, and avoids the inclusion of data non-specific to the 5-HT system. Finally, we investigate the associations between our parcellations and genetic data from the Allen Human Brain Atlas (AHBA) (Hawrylycz et al., 2012) for the genes encoding for the 5-HT receptors and transporter, for completeness, and also for MAO-A.

2. Methods

2.1. Dataset

We used data from (Beliveau et al., 2017) which includes 232 individual PET and structural MRI scans from 210 healthy subjects from the Cimbi database, which in a quality-controlled, and structured way stores the largest collections of high-resolution 5-HT neuroimaging data available (Knudsen et al., 2015). Imaging data for the receptors 5-HT_{1A} ([^{11}C]CUMI-101, n = 8), 5-HT_{1B} ([^{11}C]AZ10419369, n = 36), 5-HT_{2A} ([^{11}C]Cimbi-36, n = 29) and 5-HT_4, ([^{11}C]SB207145, n = 59) and the transporter 5-HTT ([^{11}C]DASB, n = 100) were included. For more details, e.g. regarding subject inclusion criteria, please see (Knudsen et al., 2015).

2.2. Preprocessing

The data was processed as in (Beliveau et al., 2017). Briefly, the T1-weighted structural MRI were processed with FreeSurfer (Fischl, 2012) v5.3 (FS, http://surfer.nmr.mgh.harvard.edu). The dynamic PET data was realigned and coregistered to the structural MRI using boundary-based registration (Greve and Fischl, 2009) with a weighted-sum image, and was then resampled onto the standard *fsaverage* surfaces (left and right hemisphere) and smoothed with a 10 mm full-width half maximum (FWHM) Gaussian kernel. Kinetic modeling of the time-activity curves (TAC) was performed individually at every vertex using the MRTM2 model (Ichise et al., 2003) to obtain non-displaceable binding potential (BP_{ND}) values. Finally, the BP_{ND} maps were demeaned and scaled to unit variance individually for each subject and hemisphere. In our comparison to previous clustering work, the data was preprocessed as above, but the surface smoothing was performed with an 8 mm FWHM Gaussian kernel to match the approach used by James et al. (2018). Furthermore, volume smoothing of the dynamic PET data prior to sampling on the surface was performed with 0, 2, and 4 mm FWHM Gaussian filters to test the effect of increasing PVEs. Regional BP_{ND} values used to construct correlation matrices were obtained by resampling the dynamic PET data to the surface, without smoothing, averaging the TACs within each region, and modeling the data region-wise with MRTM2.

2.3. Previous clustering methodology

To evaluate the clustering strategy of James et al. (2018), we repeated their analysis with our data. For each 5-HT target, the BP_{ND} data was first averaged across subjects and then standardized by subtracting the spatial mean across vertices and dividing by the standard deviation, resulting in a single spatial map per 5-HT target (the four receptors and the transporter). The maps are then concatenated across targets and both hemispheres were combined by concatenating the data spatially. Clustering was performed using K-means initialized with K-means++ and using 50 restarts. We used the K-means implementation from the *Scikit-learn* 0.19.1 library (Fabian et al., 2011).

The silhouette coefficient (SC) curves were quantified using the same approach as James et al. (2018). We created 100 subsets of the data. Each subset was created by randomly selecting 5 subjects for each 5-HT target and by processing them as above by taking the spatial average across subjects per target, standardizing the data, and concatenating the resulting maps across targets. For each subset, K-means clustering was performed as above for cluster numbers K from 2 to 20 as done in (James et al., 2018). The SC curves were computed for each subset and each corresponding parcellation. The mean SC curve was finally used to assess the optimal number of clusters, K. The stability of the clustering procedure was assessed using adjusted mutual information (AMI). We computed the mean AMI across every pair of the 100 parcellations (where no volume smoothing was applied) created for every K.

2.4. Our clustering approach

First, we created a mean feature map for each of the 5-HT targets using a bootstrap procedure with 10,000 resampling. For each target, bootstrap samples were created by sampling with replacement the number of available scans per target from the normalized BP_{ND} maps of individual subjects and averaging them. The mean across all bootstrap samples was taken as the bootstrap estimate of the population mean map. The bootstrap procedure was informative on the variability of the mean feature maps and allowed us to compare the variance between 5-HT targets with different numbers of subjects (e.g. 5-HT_{1A} with $n = 8$ and 5-HT_{2A} with $n = 36$), see Supplementary Fig. 1. The feature maps were then concatenated across 5-HT targets. This process was performed independently for each hemisphere. We clustered the concatenated feature maps using the image foresting transform (IFT) watershed algorithm (Lotufo and Falcao, 2002; Falcao et al., 2004) using the squared Euclidean distance to determine the cost between pairs of vertices. Initial cluster centers were obtained by clustering the features maps, concatenated spatially across both hemispheres, with K-means initialized with K-means++ and using 50 restarts. To avoid potential local optimum, the clustering steps (i.e. K-means and IFT watershed) were repeated 5 times, and the solution with the highest explained variance was kept. Parcellations with number of clusters K from 2 to 20 were thus created.

To identify an optimal number of clusters K, we computed the explained variance (EV) and SC for each parcellation. However, as it became apparent that both EV and SC were monotonically increasing or decreasing with K, respectively, we created a combined score from the two metrics to obtain a trade-off between them. This strategy is similar to the approach previously introduced by (Strother et al., 1990; Shams et al., 2015) and has the advantage of providing a solution which both fits the data well (by maximizing EV) and defines well-separated clusters (by maximizing SC). The combined score was defined as

$$\mathrm{score}(K) = \mathrm{NEV}(K) \cdot \mathrm{NSC}(K) \tag{1}$$

where NEV and NSC are normalized functions of EV and SC for every cluster K. As both EV and SC may span a different interval of their $[0, 1]$ domain, the metrics were both normalized as follow so that they contribute equally to the score

$$\mathrm{NEV}(K) = \mathrm{EV}(K) \,/\, (1 - \min(\mathrm{EV})) \tag{2}$$

$$\mathrm{NMS}(K) = \mathrm{SC}(K) \,/\, \max(\mathrm{SC}) \tag{3}$$

The optimal number of clusters K according to our score is then

obtained by max(score(K)). For additional evaluation, we have also estimated the Bayesian information criterion (BIC) (Schwarz, 1978) for all the parcellations.

The stability of our parcellation was also assessed using AMI. The full clustering process described above was repeated 10 times, where for each iteration the input PET data was resampled using stratified random sampling with replacement. We then computed the mean AMI across every pairing of the 10 resulting parcellations.

Correlation plots were created by extracting regional BP_{ND} values for each individual PET scan for each regions of the parcellation with $K = 10$, and computing the associated correlation matrix. The rows and columns of the matrices were reorganized to highlight correlated groups of regions using hierarchical clustering with average linkage implemented in *SciPy* 1.3.

2.5. Evaluation of the spatial correspondence between the 5-HT system and its underlying genetic information

We used mRNA data available from the AHBA to 1) evaluate the spatial association between 5-HT target density and mRNA levels and 2) investigate how well our parcellations could explain the spatial distribution of all 5-HT genes. Previous work by (French and Paus, 2015) provides the correspondence between each of the mRNA samples of the AHBA and the regions of the DK atlas. Here we derived a mapping from the AHBA samples to specific vertices on the *fsaverage* surface (hence applicable to any parcellation on this surface) and extracted regional average mRNA values for all available 5-HT genes: HTR1A, HTR1B, HT1D, HTR1E, HTR1F, HTR2A, HTR2B, HTR2C, HTR3A, HTR3B, HTR3C, HTR3D, HTR3E, HTR4, HTR5A, HTR6, HTR7, and SCLC6A4. Additionally, we included the gene MAOA due to the role of MAO-A in the degradation of the amine molecules, including 5-HT, and its inclusion in the parcellation presented by James and colleagues (James et al., 2018). In-depth information on the AHBA can be found at http://help.brain-map.org/display/humanbrain/Documentation.

The spatial location of all tissue samples collected in the AHBA is provided in MNI152 volume space. To obtain a correspondence from the MNI152 space to the *fsaverage* surface on which our parcellations reside, we first processed the T1-weighted image of the MNI152 brain (ICBM 2009c Nonlinear Asymmetric (Fonov et al., 2009),) with FS. Then, each vertex of the MNI152 surfaces was mapped to *fsaverage* by projecting a binary mask of each vertex (where everything is zero except that given vertex) onto *fsaverage* and finding the corresponding vertex with the highest value on the surface. Finally, every sample was matched to the closest vertex on the MNI152 white matter surface and mapped to the corresponding vertex on *fsaverage*. The match between a given probe and the MNI152 surface was restricted to vertices of the surface having the same label according to the DK atlas as assigned by (French and Paus, 2015). If a sample was located more than 10 mm away in space from any vertex of the surface with the appropriate label, then the probe was discarded; a total of 98 out of 1697 samples were thus ignored. For any given parcellation on *fsaverage*, the sample-to-cluster assignment is then performed by identifying the label of the corresponding vertex. In the AHBA, each sample contains at lest two probes for each gene. To obtain a single summary value of the mRNA level for a given gene per sample, expression values from multiple probes were average for each gene and each sample. These summary values were then normalized individually for each subject using a scaled robust sigmoid normalization proposed by (Fulcher and Fornito, 2016; Fulcher et al., 2013).

The regional mRNA levels for the parcellation with $K = 10$ were obtained using a bootstrap procedure with 1000 resamplings, where each bootstrap sample was created by randomly sampling all summary values with replacement, and computing the mean in each region. The mean regional mRNA levels were used to create spatial maps and the bootstrap samples were also used to compute the mean EV of the mRNA values for the parcellation. This procedure was applied independently to all 5-HT genes.

3. Results

3.1. Previous clustering methodology

To analyse the stability of the parcellation introduced by James and colleagues (James et al., 2018), we repeated the same clustering procedure on 100 datasets created using stratified random sampling with replacement of the input subjects. Fig. 1A presents two of these parcellations, with $K = 10$. Numerous mismatches between the two parcellations can be observed, principally along the contour of the clusters. We have used AMI as a proxy for the stability of the parcellations. Fig. 1B presents the mean pairwise AMI for all the 100 parcellations obtained for K from 2 to 20. This figure indicates that the stability is largely constant at a value of approximately 0.6 across all parcellations created with their method.

We investigated the impact of PVE by artificially increasing these effects using volume smoothing of the dynamic PET data. Population average BP_{ND} maps for 5-HT_{2A} with no smoothing and 2 and 4 mm FWHM volume smoothing are outlined in Fig. 1C. These maps highlight patterns which are accentuated when increasing PVE. The bootstrapped SC curves for the clustering obtained by applying K-means to the PET data with different levels of volume smoothing are shown in Fig. 1D. With no smoothing, the curve is monotonically decreasing for $K \leq 3$, whereas for data smoothed in the volume with 2 and 4 mm FWHM the curves followed the same pattern, but there are peaks at K equals 5 and 10, increasing with larger smoothing kernels.

3.2. Our clustering approach

Fig. 2 presents the EV, SC and scores associated with the parcellations obtained with K clusters. EV and SC were monotonically increasing or decreasing, respectively. Fig. 2A indicates that, starting with $K = 6$, our parcellations perform better than both the DK atlas and the parcellation of James and colleague in explaining the mean features maps. However, the EV of the parcellations created using the approach of (James et al., 2018) on our data was slightly, but consistently higher that the values obtained with our method. Overall, a maximum score for our method is observed at $K = 10$, making this value an optimal choice for the number of clusters. This value is also supported by the BIC curve presented in Supplementary Fig. 2. Fig. 3 presents the parcellation obtained for $K = 10$ and the associated regional 5-HT profile obtained from the mean normalized BP_{ND} maps used as input for the clustering. All subsequent *post hoc* analysis were performed with this parcellation.

Regarding the stability of our clustering, the mean pairwise AMI is 0.8. In Fig. 4 we present the BP_{ND} correlation matrices for the parcellation with $K = 10$. These correlations matrices highlight the groups of regions for which BP_{ND} values are similarly correlated across individuals.

3.3. Application to mRNA data

The bootstrapped EV for all 5-HT genes obtained with the parcellation with $K = 10$ are presented in Fig. 5. The EV for all genes was less than 0.3, with the exception of the genes HTR1A, HTR1F, and HTR2C. Bootstrapped regional mRNA values obtained using our parcellation for the genes HTR1F and HTR2C and mapped to their corresponding clusters are presented in Fig. 6.

4. Discussion

Techniques such as autoradiography do not allow for a full description of the spatial correspondence between targets of the 5-HT system, but serve well as a calibration between the PET-signal and the target density. The availability of PET radioligands for some of the 5-HT targets enables the spatial characterization of the density of these targets in high spatial details. By using a clustering approach to identify regions with homogeneous densities for each of the available targets, we have, as well

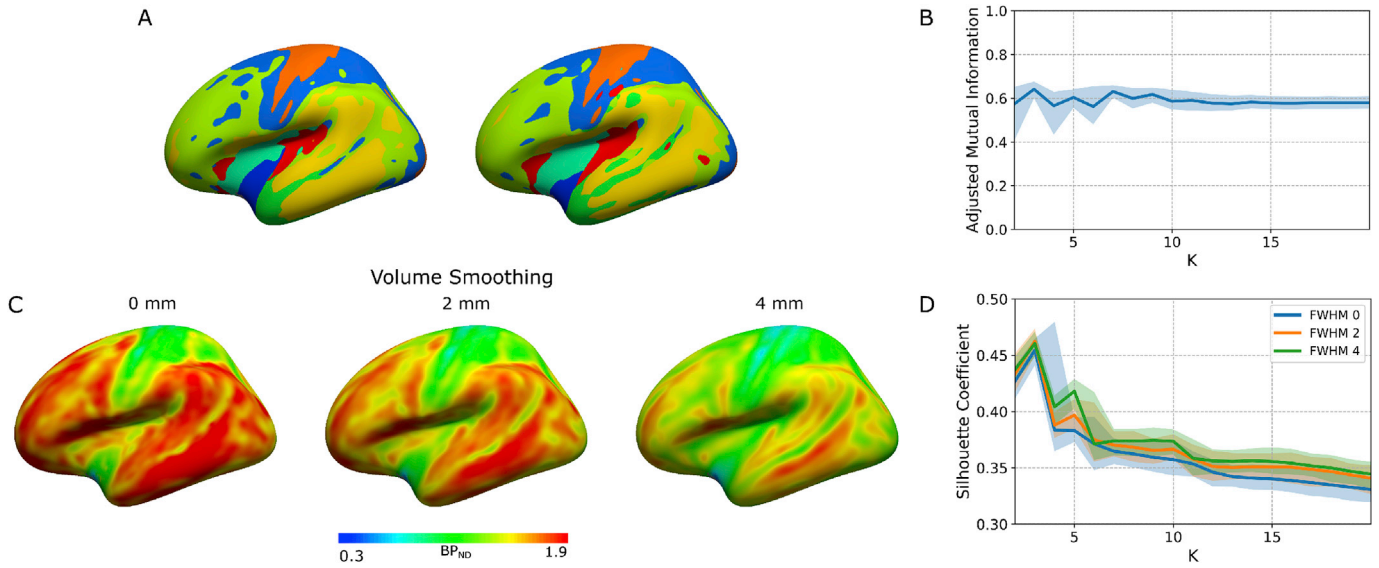

Fig. 1. (A) Parcellations obtained with K-means on two datasets created using stratified random sampling with replacement (no volume smoothing), (B) adjusted mutual information (AMI) across all pairs of 100 parcellations obtained for every K, (C) the effect of volume smoothing on the BP_{ND}, (D) silhouette coefficient (SC) curve for the clustering obtained from data volume smoothed at 0 mm, 2 mm and 4 mm FWHM. Data in A and C are displayed on a lateral view of the *fsaverage* surface (left hemisphere, inflated). In B and D, solid lines are mean values and shaded areas are the corresponding 95% confidence interval.

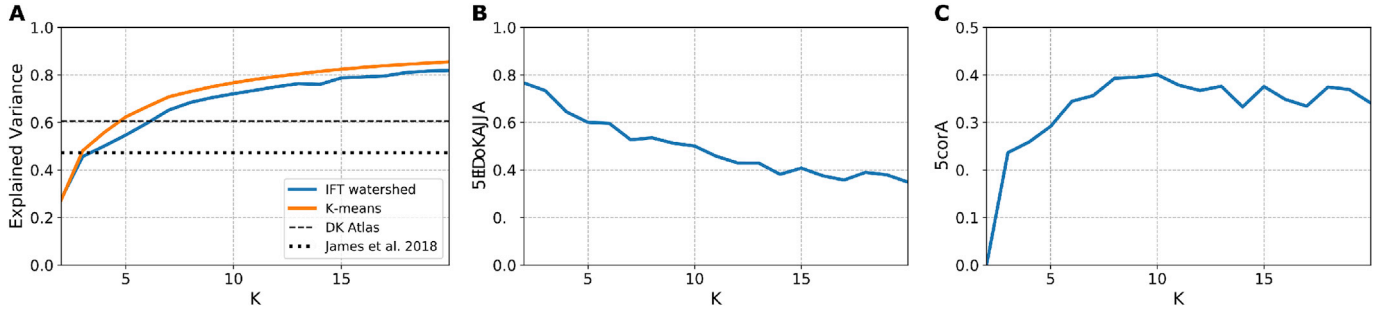

Fig. 2. (A) Explained variance (EV), (B) Silhouette coefficient (SC), and (C) score combining normalized EV and SC for parcellations created with our clustering approach (IFT-watershed). As comparison, we have also included in (A) the EV for the parcellations created when using the approach suggested by (James et al., 2018) (K-means) on our data, the parcellation reported by (James et al., 2018), and the DK atlas.

as a previous study (James et al., 2018), attempted to identify the overall spatial organization characterizing the 5-HT system.

Overall, our parcellations can explain the underlying molecular imaging data better than previous parcellations. This is not entirely surprising as those parcellations were derived from different underlying data. Fig. 2A indicates that with $K = 10$, our parcellation can explain between 10 and 20% more variation in the data compared to the DK atlas and the parcellation from James and colleagues, suggesting that it reflects the underlying spatial organization of the 5-HT system more accurately. However, it also indicates that the parcellation obtained with K-means can explain approximately 4% more variation in the data. Nonetheless, our parcellation exhibits a higher stability, as captured by a higher AMI (0.8 vs. 0.6), compared to the parcellation obtained with K-means, and represents a better trade-off between model fit and stability.

The correlation matrices presented in Fig. 4 reveal that the density of the receptors $5\text{-}HT_{1A}$, $5\text{-}HT_{1B}$, and $5\text{-}HT_{2A}$ is highly correlated across most brain regions, although less for $5\text{-}HT_4$ and 5-HTT, suggesting an almost brain wide involvement of 5-HT for all 5-HT targets studied here. Cluster 7, corresponding to parahippocampal gyrus, appears to have a weaker association to all other brain regions for all 5-HT targets and is likely capturing non-biological signal such as PVE.

The 5-HT profiles outlined in Fig. 3 provide information regarding the specific involvement of the 5-HT targets across cortex. These association can potentially be useful for guiding *a priori* hypotheses of pharmacological interventions. It is interesting to note that all 5-HT targets appears to have approximately average levels within the clusters 1, 8, 9, and 10 (i.e. the mean normalized BP_{ND} being close to 0 for all targets) suggesting that 5-HT may possibly have a more general role in these regions, rather than primarily targeting a specific subset of receptors. This is again supported by the widespread correlation between most regions exhibited in Fig. 4.

4.1. Previous clustering methodology

In the first part, we evaluated the clustering approach proposed by James et al. (2018) on our data. PVE is a known and important challenge intrinsic to the processing of PET data. Initial work on the surface-based processing of PET data has outlined stripe-like patterns following the cortical sulci due to PVE (Greve et al., 2014), and these patterns were present in the clustering obtained by James and colleagues. Here we show that when we artificially increase PVE by spatial smoothing, these patterns are accentuated, further supporting that PVE induces artifacts in a parcellation (Fig. 1C). Even with our high-resolution PET data, PVE may still be an issue, however, we used a larger surface smoothing kernel (10 mm instead of 8 mm) to mitigate these effects. Although our high-resolution PET data still contains smaller PVE effects, we opted not

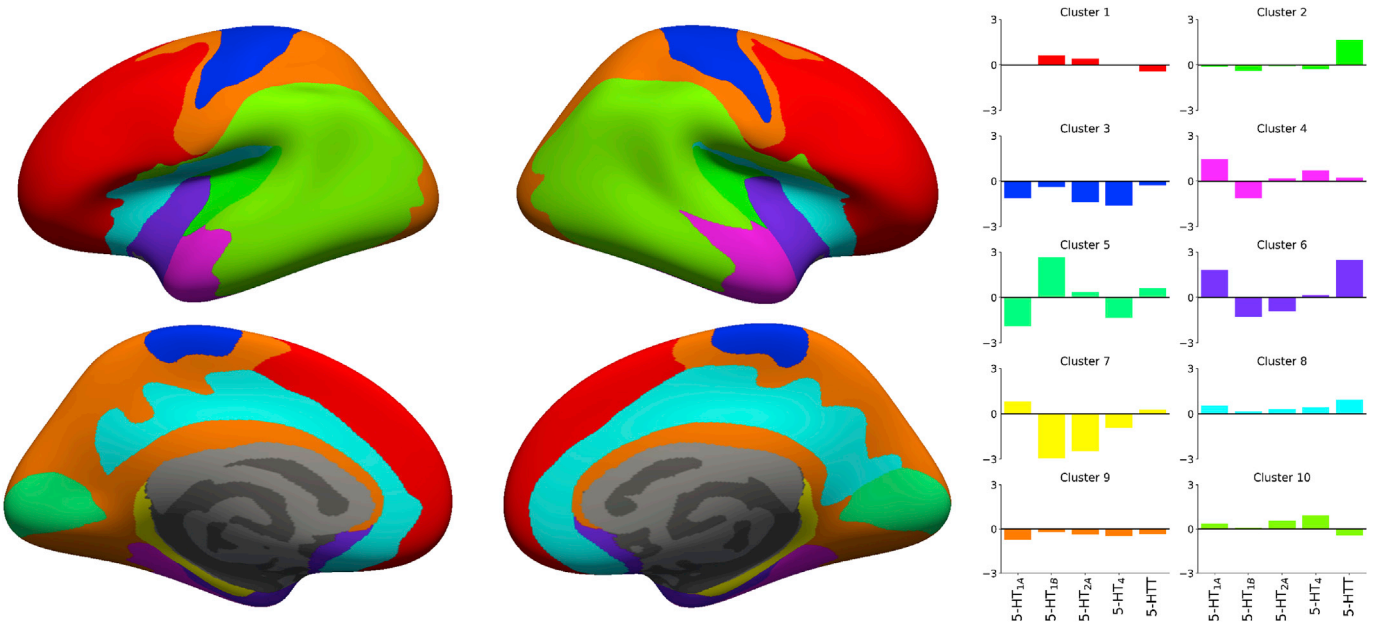

Fig. 3. Parcellation obtained with $K = 10$ and the associated regional 5-HT profile for each region. The parcellation is presented on the inflated *fsaverage* surface medial (lower) and lateral (upper) for both hemisphere (left and right).

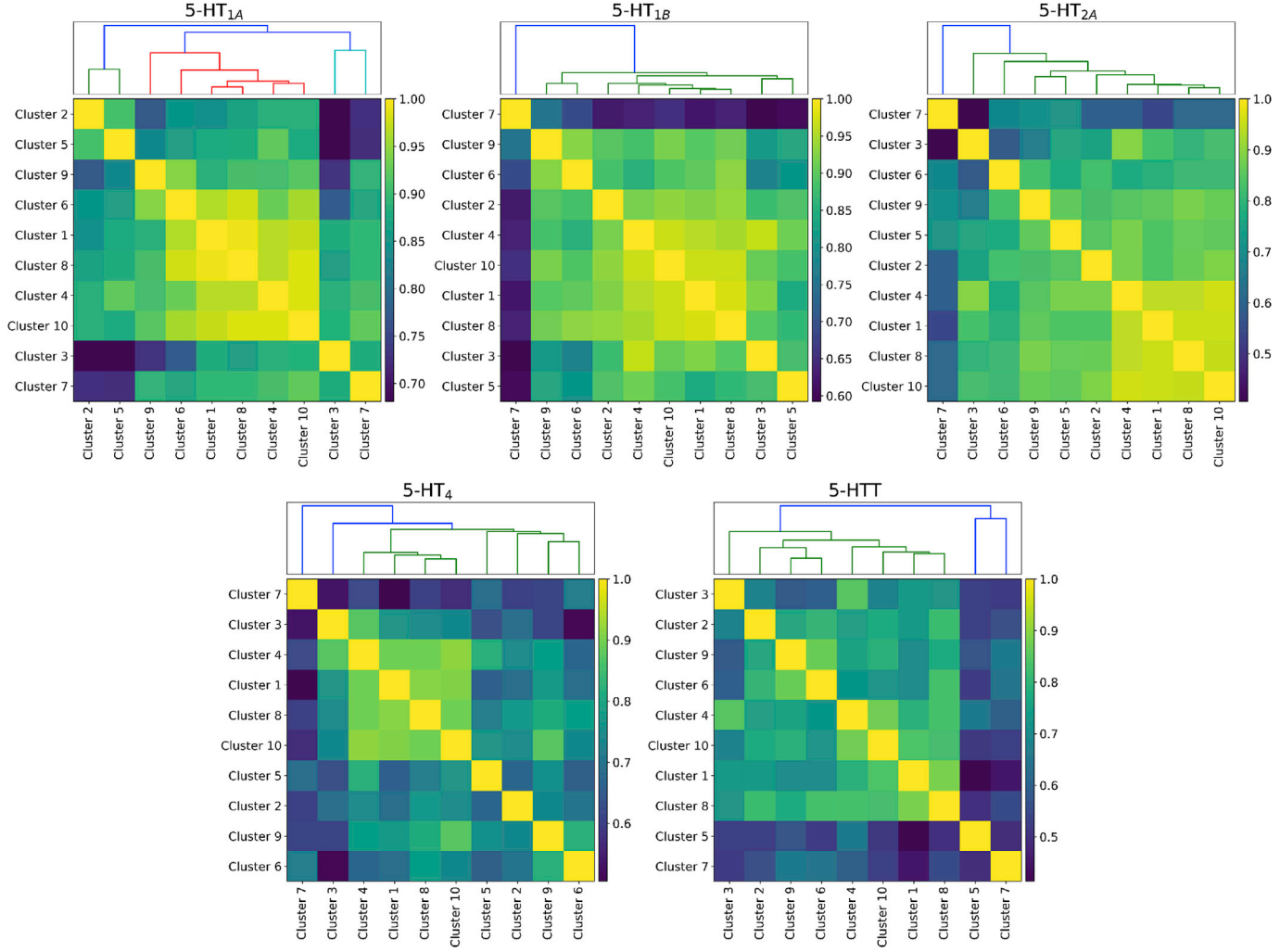

Fig. 4. BP_{ND} correlation matrices for each 5-HT target. Matrices were reorganized using hierarchical clustering and the associated dendrograms presented above their corresponding matrix.

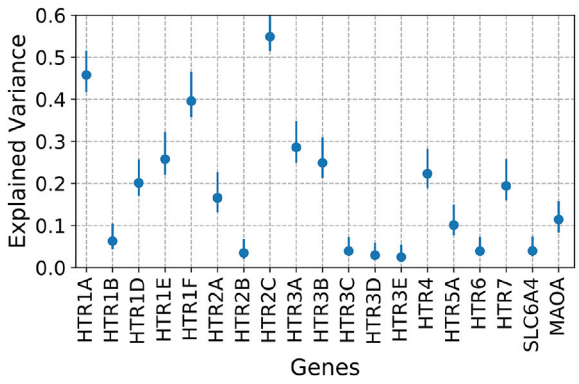

Fig. 5. Bootstrapped explained variance (EV) for the parcellation with $K = 10$ across all 5-HT genes. Error bars correspond to the 95% confidence intervals.

to use PVC to avoid introducing a systematic bias due to violation of the PVC assumptions, e.g. constant point spread function throughout the field of view of the scanner and homogeneous tracer distribution within all regions of interest (Thomas et al., 2011; Erlandsson et al., 2012). This is consistent with the 5-HT atlas previously published based on the same data (Beliveau et al., 2017).

One of the main challenges in clustering and subsequent selection of the optimal number of clusters is that of stability. James and colleagues have used the K-means algorithm directly to cluster their data. As exemplified in Fig. 1A and B if the input consists of slightly different data this will results in different parcellations, hence that specific solution cannot be considered stable. This is also reflected by an AMI that is 25% lower compared to our data.

It is important to note that choosing the optimal number of clusters remains a heuristical choice, whatever the metric being used, and that multiple factors may have to be considered when selecting a parcellation to be used with an external dataset, e.g. image resolution. On this particular issue, James and colleagues have identified an optimal number of clusters $K = 5$. Our results with volume-smoothed data indicate that PVE creates a bias which increases the SC values, and especially for clustering with $K = 5$ and 10 (Fig. 1A and B), suggesting that $K = 5$ may be an optimum only in the presence of PVE.

4.2. Application to mRNA data

We have investigated how well our parcellation could explain the mRNA data of all 5-HT genes. It is important to keep in mind that the spatial resolution of the mRNA data is an order of magnitude lower than that of PET data as only a few hundred samples are collected throughout the whole of neocortex per subject. Also, samples were collected from only 6 subjects, and from both hemispheres for only two of those. Although the spatial distribution of all 5-HT targets to some extent has been previously described (Muller and Jacobs, 2009), others yet remain to be studied *in vivo* due to the lack of specific radioligands which means that their precise spatial distribution within the human brain remains unknown. The 5-HT_{1A}R/HTR1A has consistently been shown to have a strong spatial correlation between the density of the receptor and the underlying mRNA levels (Savli et al., 2012; Beliveau et al., 2017). Our parcellation achieved EV comparable or higher to that of HTR1A only for the HTR1F and HTR2C genes. Interestingly, previous results also suggest a good spatial correspondence between receptor density and mRNA levels in the neocortex of rodents and monkeys for 5-HT_{1F}R/HTR1F and 5-HT_{2C}R/HTR2C (López-Giménez et al., 2000; Mengod et al., 2010; Waeber and Moskowitz, 1995). As such, the regional mRNA levels presented in Fig. 6 for the genes HTR1F and HTR2C form a putative representation of the spatial density for the corresponding receptors. Finally, we note that our parcellation could not explain the spatial distribution of MAO-A levels within neocortex, which further questions the validity of using MAO-A to describe the 5-HT system.

4.3. Limitations

Although we evaluated the association between our parcellations and genetic information, we were not able to establish a clear biological validation of our results. Our new 5-HT parcellation introduces a set of regions which can explain the 5-HT molecular imaging data better compared to the DK atlas and the parcellation from James and colleagues. Furthermore, it contains substantially less regions than the DK atlas, which results in a less stringent correction for multiple comparisons when using this parcellation in a subsequent statistical analysis. This suggest that our new parcellation may be better suited to detect biological changes related to 5-HT modulation. However, we were not able to obtain a dataset where this could be exemplified.

The small sample size ($n = 8$) for the 5-HT_{1A} receptor may potentially bias the clustering if some of the subjects deviate largely from the population mean. However, the variation of the mean normalized BP_{ND} estimates for this receptor (see Supplementary Fig. 1) is comparable to that of other receptors (e.g. 5-HT_{2A}), hence, we have no evidence for this in our data.

5. Conclusion

We provide a new parcellation describing the spatial organization of the 5-HT system within neocortex. This parcellation provides a more accurate description of 5-HT molecular imaging data compared to previous atlases. We have assessed how well this parcellation can capture

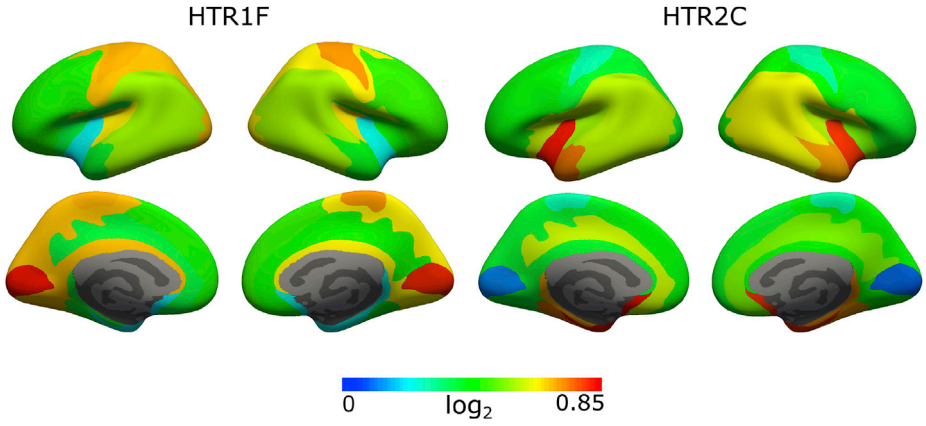

Fig. 6. Bootstrapped regional mRNA levels for the genes *HTR1F* and *HTR2C* obtained from the parcellation with $K = 10$. Values are presented on the inflated *fsaverage* surface medial (lower) and lateral (upper) for both hemisphere (left and right).

the spatial organization of the genetic information for all 5-HT genes. This work furthers our understanding of the structure of the 5-HT system and the new parcellation forms a tool which may potentially be more sensitive to regional changes modulated by 5-HT compare to other atlases. The parcellation is available at https://xtra.nru.dk/FS5ht-atlas/.

Declaration of competing interest

G.M.K. has served as a consultant for Sage Therapeutics and is a stock holder of Novo Nordisk/Novozymes. S.S. is the consulting Chief Scientific Officer at ADMdx, Inc. V.B., B.O., D.N.G., C.S and M.G. have no conflict of interest to report.

Acknowledgements

V.B. was supported by the Independent Research Fund Denmark [DFF-4183-00627]. B.O. was supported by the Lundbeck foundation [R231-2016-3236] and Marie-Curie-NEUROMODEL. S.S. is partly supported by grants from the Ontario Brain Institute and by a CIHR Operating Grant [MOP 201403]. D.N.G was supported by NIH grant [R01 EB023281-01]. M.G. was supported by the Lundbeck foundation [R181-2014-3586] as well. We thank Gael Varoquaux for fruitful discussions.

Appendix A. Supplementary data

Supplementary data to this article can be found online at https://doi.org/10.1016/j.neuroimage.2019.116240.

References

Beliveau, V., Ganz, M., Feng, L., Ozenne, B., Højgaard, L., Fisher, P.M., Svarer, C., Greve, D.N., Knudsen, G.M., 2017. "A high-resolution in vivo atlas of the human brain's serotonin system. J. Neurosci. vol. 37 (1), 120–128.

Broadman, K., 1909. Vergleichende Lokalisationslehre der Grosshirnrinde. Barth, Leipzig, Germany [Title translation: Comparative study of localization in the cerebral cortex.].

Desikan, R.S., Ségonne, F., Fischl, B., Quinn, B.T., Dickerson, B.C., Blacker, D., Buckner, R.L., Dale, A.M., Maguire, R.P., Hyman, B.T., Albert, M.S., Killiany, R.J., 2006. An automated labeling system for subdividing the human cerebral cortex on MRI scans into gyral based regions of interest. Neuroimage vol. 31 (3), 968–980.

Erlandsson, K., Buvat, I., Pretorius, P.H., Thomas, B.a., Hutton, B.F., 2012. A review of partial volume correction techniques for emission tomography and their applications in neurology, cardiology and oncology. Phys. Med. Biol. vol. 57 (21), R119–R159.

Fabian, Pedregosa, Michel, V., Grisel, O., Blondel, M., Prettenhofer, P., Weiss, R., Vanderplas, J., Cournapeau, D., Pedregosa, F., Varoquaux, G., Gramfort, A., Thirion, B., Grisel, O., Dubourg, V., Passos, A., Brucher, M., Perrot, M., Duchesnay, d., 6 2011. Scikit-learn: machine learning. J. Mach. Learn. Res. Vol. 12, 2825–2830.

Falcao, A., Stolfi, J., de Alencar Lotufo, R., 1 2004. The image foresting transform: theory, algorithms, and applications. IEEE Trans. Pattern Anal. Mach. Intell. Vol. 26, 19–29.

Fischl, B., 2012. FreeSurfer. Neuroimage vol. 62 (2), 774–781.

Fonov, V., Evans, A., McKinstry, R., Almli, C., Collins, D., 2009. Unbiased nonlinear average age-appropriate brain templates from birth to adulthood. Neuroimage vol. 47, S102, 7.

French, L., Paus, T., 2015. A FreeSurfer view of the cortical transcriptome generated from the allen human brain atlas. Front. Neurosci. Vol. 9 (September), 1–5.

Fulcher, B.D., Fornito, A., 2016. A transcriptional signature of hub connectivity in the mouse connectome. Proc. Natl. Acad. Sci. vol. 113 (5), 1435–1440.

Fulcher, B.D., Little, M.A., Jones, N.S., 2013. Highly comparative time-series analysis: the empirical structure of time series and their methods. J. R. Soc. Interface Vol. 10, 4, 20130048-20130048.

Greve, D.N., Fischl, B., 2009. Accurate and robust brain image alignment using boundary-based registration. Neuroimage vol. 48, 63–72, 10.

Greve, D.N., Svarer, C., Fisher, P.M., Feng, L., Hansen, A.E., Baare, W., Rosen, B., Fischl, B., Knudsen, G.M., 2014. Cortical surface-based analysis reduces bias and variance in kinetic modeling of brain PET data. Neuroimage 92C, 225–236, 12.

Hawrylycz, M.J., Lein, E.S., Guillozet-Bongaarts, A.L., Shen, E.H., Ng, L., Miller, J.A., van de Lagemaat, L.N., Smith, K.A., Ebbert, A., Riley, Z.L., Abajian, C., Beckmann, C.F., Bernard, A., Bertagnolli, D., Boe, A.F., Cartagena, P.M., Chakravarty, M.M., Chapin, M., Chong, J., Dalley, R.A., Daly, B.D., Dang, C., Datta, S., Dee, N., Dolbeare, T.A., Faber, V., Feng, D., Fowler, D.R., Goldy, J., Gregor, B.W., Haradon, Z., Haynor, D.R., Hohmann, J.G., Horvath, S., Howard, R.E., Jeromin, A., Jochim, J.M., Kinnunen, M., Lau, C., Lazarz, E.T., Lee, C., Lemon, T.A., Li, L., Li, Y., Morris, J.A., Overly, C.C., Parker, P.D., Parry, S.E., Reding, M., Royall, J.J., Schulkin, J., Sequeira, P.A., Slaughterbeck, C.R., Smith, S.C., Sodt, A.J., Sunkin, S.M., Swanson, B.E., Vawter, M.P., Williams, D., Wohnoutka, P., Zielke, H.R., Geschwind, D.H., Hof, P.R., Smith, S.M., Koch, C., Grant, S.G.N., Jones, A.R., 2012. An anatomically comprehensive atlas of the adult human brain transcriptome. Nature Vol. 489 (7416), 391–399.

Ichise, M., Liow, J.-S., Lu, J.-Q., Takano, A., Model, K., Toyama, H., Suhara, T., Suzuki, K., Innis, R.B., Carson, R.E., 9 2003. Linearized reference tissue parametric imaging methods: application to [11 C]DASB Positron emission tomography studies of the serotonin transporter in human brain. J. Cereb. Blood Flow Metab. vol. 23, 1096–1112.

James, G.M., Gryglewski, G., Vanicek, T., Berroterán-Infante, N., Philippe, C., Kautzky, A., Nics, L., Vraka, C., Godbersen, G.M., Unterholzner, J., Sigurdardottir, H.L., Spies, M., Seiger, R., Kranz, G.S., Hahn, A., Mitterhauser, M., Wadsak, W., Bauer, A., Hacker, M., Kasper, S., Lanzenberger, R., 2018. Parcellation of the human cerebral cortex based on molecular targets in the serotonin system quantified by Positron emission tomography in vivo. Cerebr. Cortex 10, 1–11.

Kalbitzer, J., Svarer, C., 2009. A probabilistic approach to delineating functional brain regions. J. Nucl. Med. Technol. 37, 91–95, 6.

Knudsen, G.M., Jensen, P.S., Erritzoe, D., Baaré, W.F., Ettrup, A., Fisher, P.M., Gillings, N., Hansen, H.D., Hansen, L.K., Hasselbalch, S.G., Henningsson, S., Herth, M.M., Holst, K.K., Iversen, P., Kessing, L.V., Macoveanu, J., Madsen, K.S., Mortensen, E.L., Nielsen, F.r., Paulson, O.B., Siebner, H.R., Stenbæk, D.S., Svarer, C., Jernigan, T.L., Strother, S.C., Frokjaer, V.G., 4 2015. The center for integrated molecular brain imaging (Cimbi) database. Neuroimage Vol. 124, 1213–1219.

López-Giménez, J.F.J., Vilaró, M.T., Palacios, J.M.J.M., Mengod, G., Vilaro, T.M., Palacios, J.M.J.M., Mengod, G., 2000. Mapping of 5-HT2A receptors and their mRNA in monkey brain: [3H]MDL100,907 autoradiography and in situ hybridization studies. J. Comp. Neurol. vol. 429, 571–589, 2001.

Lotufo, R., Falcao, A., 2002. The ordered queue and the optimality of the watershed approaches. In: Mathematical Morphology and its Applications to Image and Signal Processing. Kluwer Academic Publishers, Boston, pp. 341–350.

Mengod, G., Cortés, R., Vilaró, M.T., Hoyer, D., 2010. Distribution of 5-HT receptors in the central nervous system. In: Handbook of Behavioral Neuroscience, vol. 21. Elsevier, pp. 123–138.

Muller, C.P., Jacobs, B., 2009. Handbook of the Behavioral Neurobiology of Serotonin, vol. 21. Academic Press.

Savli, M., Bauer, A., Mitterhauser, M., Ding, Y., 10 2012. Normative database of the serotonergic system in healthy subjects using multi-tracer PET. Neuroimage Vol. 63, 447–459.

Schwarz, G., 3 1978. Estimating the dimension of a model. Ann. Stat. Vol. 6, 461–464.

Shams, S.-M., Afshin-Pour, B., Soltanian-Zadeh, H., Hossein-Zadeh, G.-A., Strother, S.C., 9 2015. Automated iterative reclustering framework for determining hierarchical functional networks in resting state fMRI. Hum. Brain Mapp. 36, 3303–3322.

Strother, S., Oder, A., Spring, R., Grady, C., 1990. The NPAIRS Computational Statistics Framework for Data Analysis in Neuroimaging. il. Development, pp. 1–9, 2002.

Svarer, C., Madsen, K., Hasselbalch, S.G., Pinborg, L.H., Haugbøl, S., Frøkjær, V.G., Holm, S., Paulson, O.B., Knudsen, G.M., 2005. MR-based automatic delineation of volumes of interest in human brain PET images using probability maps. Neuroimage vol. 24 (4), 969–979.

Thomas, B.A., Erlandsson, K., Modat, M., Thurfjell, L., Vandenberghe, R., Ourselin, S., Hutton, B.F., 2011. "The importance of appropriate partial volume correction for PET quantification in Alzheimer's disease. Eur. J. Nucl. Med. Mol. Imaging vol. 38, 1104–1119, 6.

Tzourio-Mazoyer, N., Landeau, B., Papathanassiou, D., Crivello, F., Etard, O., Delcroix, N., Mazoyer, B., Joliot, M., 1 2002. Automated anatomical labeling of activations in SPM using a macroscopic anatomical parcellation of the MNI MRI single-subject brain. Neuroimage vol. 15, 273–289.

Varnäs, K., Halldin, C., Hall, H., 2004. Autoradiographic distribution of serotonin transporters and receptor subtypes in human brain. Hum. Brain Mapp. Vol. 22, 246–260, 7.

Waeber, C., Moskowitz, M.A., 1995. [3H]sumatriptan labels both 5-HT1D and 5-HT1F receptor binding sites in the Guinea pig brain: an autoradiographic study. Naunyn Schmiedeberg's Arch. Pharmacol. vol. 352, 263–275, 9.